Electronic Structure and Symmetry in Nickel L Edge X-ray Absorption Spectroscopy: Application to a Nickel Protein

J. van Elp,[†] G. Peng,[‡] B. G. Searle,[§] S. Mitra-Kirtley,[∥] Y.-H. Huang,[⊥] M. K. Johnson,[⊥] Z. H. Zhou,[#] M. W. W. Adams,[#] M. J. Maroney,[▽] and S. P. Cramer*[,†,‡]

Contribution from Energy and Environment Division, Lawrence Berkeley Laboratory, Berkeley, California 94720, Department of Applied Science, University of California at Davis, Davis, California 95616, SERC Daresbury Laboratory, Warrington WA4 4AD U.K., Department of Physics and Applied Optics, Rose-Hulman Institute of Technology, 5500 Wabash Avenue, Terre Haute, Indiana 47803, Departments of Chemistry and Center for Metalloenzyme Studies and Biochemistry and Center for Metalloenzyme Studies, University of Georgia, Athens, Georgia 30602, Department of Chemistry, University of Massachusetts, Amherst, Massachusetts 01003

Received September 20, 1993[●]

Abstract: We have studied the effects of electronic structure and symmetry on Ni $L_{2,3}$ edge X-ray absorption spectra by measuring the $L_{2,3}$ edges of several nickel compounds with different structural symmetries. Using ligand field atomic multiplet calculations, we find that there is a close relationship between the Ni $L_{2,3}$ edge spectral features and the electronic structure at the nickel site. The $L_{2,3}$ absorption edge is very sensitive to the spin state and the oxidation state of the nickel site, even for the formally trivalent nickel oxidation state. The Ni $L_{2,3}$ edge is also sensitive to different structural nickel site symmetries, but less sensitive to changes in individual ligands. In the protein system investigated, the Ni-substituted *Pyrococcus furiosus* rubredoxin, we find a strongly distorted T_d symmetry and a large zero field splitting, comparable to that observed in an optical MCD study. Because of the chemical sensitivity and specificity for only the nickel site, Ni $L_{2,3}$ edges are a strong spectroscopic tool for investigating the nickel sites in large metalloproteins. The information obtained at the Ni $L_{2,3}$ edge complements information from EXAFS measurements at the nickel K edge.

Introduction

The role of Ni as an important element in biochemistry is clear from its occurrence in at least four enzymes: hydrogenase, CO dehydrogenase, methyl-S-coenzyme-M reductase, and urease.[1] In the Ni hydrogenases and the CO dehydrogenases the local Ni geometry is not well-defined, and the different Ni oxidation states in the catalytic cycle are not fully understood.[1] In this paper we show the sensitivity of Ni $L_{2,3}$ edge X-ray absorption spectroscopy (XAS) to electronic structure and symmetry using a variety of Ni compounds with different structures. The Ni $L_{2,3}$ edge is then used to investigate the Ni site in Ni-substituted *Pyrococcus furiosus* rubredoxin, a protein whose EPR signals of the ferricyanide oxidized form[2] show a striking similarity with the EPR signals of the Ni-C form in Ni hydrogenases. The Fe $L_{2,3}$ edges of the native form of this rubredoxin have been reported.[3] The main question which we want to address in this paper is what information can we obtain by using Ni $L_{2,3}$ edges XAS for studying the nickel sites in metalloproteins as well as nickel model compounds.

The 3d transition metal $L_{2,3}$ edges are $2p \rightarrow 3d$ dipole-allowed transitions located in the soft X-ray region (400–1000 eV). They have 3–4 times smaller line widths than the near-edge region of the corresponding 3d transition metal K edges, allowing observation of sharp multiplet structures at the $L_{2,3}$ edges. The 3d transition metal $L_{2,3}$ edges are in general sensitive to oxidation state, spin state, and ligand field changes.[4-6] They can be interpreted by established theoretical procedures based on a ligand field atomic multiplet calculation,[5] in which interactions between the 2p core hole and the 3d valence electrons are taken into account. The $L_{2,3}$ edges, as described by $3d^n \rightarrow \underline{2p}3d^{n+1}$ (where $\underline{2p}$ stands for the 2p core hole) transitions, show a spectrum consisting of a "fingerprint" of available final states for every $3d^n$ initial state.

The information obtained from these $L_{2,3}$ edge spectra is different from the information obtained from the EXAFS region of the corresponding K edges, where the extended X-ray absorption fine structure gives information about bond distances and ligand coordination numbers. Furthermore, $L_{2,3}$ edge XAS is of course element specific as compared to UV–visible or EPR spectroscopy or magnetic susceptibility measurements.

The Ni $L_{2,3}$ edge has been studied with high resolution before, using a double-crystal monochromator equipped with beryl crystals, and large differences were observed between triplet high spin and singlet low spin divalent Ni compounds.[7] Also, charge-transfer effects (from the ligand valence orbitals to the Ni 3d orbitals) have been investigated in the Ni dihalides,[8] and a consistent change in spectral features depending on the halide electronegativity was observed. Similar to the hole-doping behavior of the new class of Cu-based high-T_c superconductors,

† Lawrence Berkeley Laboratory.
‡ University of California at Davis.
§ SERC Daresbury Laboratory.
∥ Rose-Hulman Institute of Technology.
⊥ Department of Chemistry and Center for Metalloenzyme Studies, University of Georgia.
Department of Biochemistry and Center for Metalloenzyme Studies, University of Georgia.
▽ University of Massachusetts.
● Abstract published in *Advance ACS Abstracts*, February 1, 1994.

(1) *The Bioinorganic Chemistry of Nickel*; Lancaster, J. R., Ed.; VCH Publishers, Inc.: New York, 1988.
(2) Huang, Y.-H.; Park, J.-B.; Adams, M. W. W.; Johnson, M. K. *Inorg. Chem.* **1993**, *32*, 375–376.
(3) George, S. J.; van Elp, J.; Chen, J.; Ma, Y.; Chen, C. T.; Park, J.-B.; Adams, M. W. W.; Searle, B. G.; de Groot, F. M. F.; Fuggle, J. C.; Cramer, S. P. *J. Am. Chem. Soc.* **1992**, *114*, 4426–4427.
(4) Thole, B. T.; Cowan, R. D.; Sawatzky, G. A.; Fink, J.; Fuggle, J. C. *Phys. Rev. B* **1985**, *31*, 6856–6858.
(5) van der Laan, G.; Kirkwood, I. W. *J. Phys.: Condens. Matter* **1992**, *4*, 4189–4204.
(6) Cramer, S. P.; de Groot, F. M. F.; Ma, Y.; Chen, C. T.; Sette, F.; Kipke, C. A.; Eichhorn, D. M.; Chan, M. K.; Armstrong, W. H.; Libby, E.; Christou, G.; Brooker, S.; McKee, V.; Mullins, O. C.; Fuggle, J. C. *J. Am. Chem. Soc.* **1991**, *113*, 7937–7940.
(7) van der Laan, G.; Thole, B. T.; Sawatzky, G. A.; Verdaguer, M. *Phys. Rev. B* **1988**, *37*, 6587–6589.
(8) van der Laan, G.; Zaanen, J.; Sawatzky, G. A.; Karnatak, R.; Esteva, J.-M. *Phys. Rev. B* **1986**, *33*, 4253–4263.

0002-7863/94/1516-1918$04.50/0

where the hole-doped state is mainly a $d^9\underline{L}$ state (where $\underline{L}$ stands for a hole in the ligand (oxygen) band) instead of a d^8 state, it was shown, using first the oxygen K edge[9] and later on confirmed at the Ni $L_{2,3}$ edge[10], that the charge compensating states upon hole doping in $Li_xNi_{1-x}O$ are of primarily O 2p character (mainly $d^8\underline{L}$). Although the charge-compensating states are mainly of oxygen character, the $L_{2,3}$ spectral features do change.

However, information on the local nickel symmetry obtained from Ni $L_{2,3}$ edges experiments has not been reported. In this paper we investigate the sensitivity of Ni $L_{2,3}$ edges to electronic structure and symmetry for a variety of nickel complexes.

Experimental Section

Preparation of Model Compounds. The following samples were prepared according to the published procedures:[11] $[Ni(tren)_2](BF_4)_2$,[12] $[Ni(ttcn)_2](BF_4)_2$,[13] Ni(cyclam)Cl_2,[14] Ni(salen),[15] $[Ni(cyclam)](ClO_4)_2$,[14] $(Ph_4As)_2[Ni(NCS)_4]$,[16] and $[Ni(cyclam)Cl_2]ClO_4$.[17] The less stable samples were recrystallized shortly before the measurements and stored under dry nitrogen. Fresh surfaces of the compounds were prepared by grinding the samples in an anaerobic glovebox. The powders were attached to a Cu sample holder using double-sided adhesive tape.

Preparation of Ni-Substituted Rubredoxin. *P. furiosus* rubredoxin was purified using published procedures.[18] Preparation of the apoprotein and subsequent reconstitution with nickel were performed as described.[19] Oxidation by ferricyanide in the presence of excess cyanide results in a sharp, slowly relaxing, axial $S = 1/2$ EPR signal.[2] The spin quantitation depends on the ferricyanide and cyanide concentrations and is maximal at ~0.3 spin/molecule for the oxidized Ni rubredoxin.[2] Samples of the as-prepared and ferricyanide-oxidized forms of Ni rubredoxin for the $L_{2,3}$ edge experiment were prepared as partially dehydrated thin films, made in an anaerobic glovebox by placing about 0.1 mL of a 5.0 mM protein solution in 10 mM Tris buffer, pH 8.0, on a silicon slide.

$L_{2,3}$ Edge XAS Experiments. The Ni $L_{2,3}$ edge XAS spectra were recorded on AT&T beamline U4B[20] at the National Synchrotron Light Source, Brookhaven National Laboratory. A refocusing mirror produced a focused beam spot (1 mm × 1.5 mm) on the sample. The photon energy resolution was set at 350 meV. The main chamber was maintained at a vacuum of less then 2×10^{-9} mbar. From the glovebox the samples were anaerobically introduced into the loadlock. After evacuation of the loadlock, the samples were transferred to the main chamber and mounted on a precooled <10 K cold finger attached to a liquid helium flow cryostat. The Ni $L_{2,3}$ edges of the model compounds were measured using total electron yield. No charging effects in the model spectra were observed. X-ray fluorescence from all the samples was detected using a windowless 13-element germanium detector.[21] By using fluorescence detection, we can electronically resolve the Ni L edge fluorescence from the mainly oxygen Kα background, improving the base-line stability and signal to noise ratio. All the Ni $L_{2,3}$ edge spectra were calibrated using the spectrum of NiF_2, which has an absorption maximum at 852.7 eV.[8] The spectra were normalized to the incident flux as observed with a total electron yield signal from a high-permeability gold-coated grid positioned between monochromator and refocusing mirror. To allow for a good comparison with the theoretical 3d absorption spectral weight, in all the model compounds the background is subtracted by fitting a polynomial function to the data in a region in front of the L_3 edge and beyond the L_2 edge. The Ni-substituted rubredoxin is shown as measured after beam current normalization. Comparison of data from several scans showed no photoreduction or radiation damage in the Ni-substituted rubredoxin, nor in any of the model compounds.

Ligand Field Atomic Multiplet Calculations. The calculations describe the transition for a divalent Ni ion from a $3d^8$ ground state to $2p3d^9$ (where $\underline{2p}$ stands for the 2p core hole) final states. First, initial state (F^2_{dd} and F^4_{dd}) and final state (F^2_{pd}, G^1_{pd}, and G^1_{pd}) Coulomb and exchange interactions and 2p and 3d spin orbit interactions are calculated. Charge-transfer effects in the calculations are taken into account by a reduction of the *ab initio* Hartree–Fock values of the Coulomb and exchange integrals. For the 3d transition metals the tabulated free atom values of Griffith[22] for the 3d Coulomb integrals are comparable to the Hartree–Fock *ab initio* calculated values reduced to 89% of their initial values. To describe the local symmetry a ligand field splitting is added as an adjustable parameter. In O_h (T_d) symmetry the 3d orbitals are split into e_g (e) and t_{2g} (t_2) orbitals with an energy difference $10Dq$. In lowering the symmetry to D_{4h} (D_{2d}) the orbitals are further split by the ligand field parameter Ds. The parameters ($10Dq$ and Ds) are obtained from a fit to the experimental spectrum and are final-state parameters. The calculated spectra are broadened with a Lorentzian (linewidth: 2Γ eV (fwhm)) and convoluted with a σ eV wide Gaussian, to describe the lifetime and instrumental broadening processes present.[23] The *ab initio* Hartree–Fock values of the Slater integrals and spin–orbit couplings (2p and 3d) are used as tabulated.[5]

The parameters and symmetries used in the calculations are as follows. $[Ni(tren)_2](BF_4)_2$: O_h symmetry, $[NiN_6]$ site, $10Dq = 1.5$ eV, Slater integrals at 70%, $\sigma = 0.3$ eV, $\Gamma = 0.25$ (0.35) eV for L_3 (L_2) edge. $[Ni(ttcn)_2](BF_4)_2$: O_h symmetry, $[NiS_6]$ site, $10Dq = 0.75$ eV, Slater integrals at 40%, $\sigma = 0.25$ eV, $\Gamma = 0.25$ (0.50) eV. Ni(cyclam)Cl_2: D_{4h} symmetry, $[NiN_4Cl_2]$ site, $10Dq = 1.6$ eV, $Ds = 0.22$ eV, Slater integrals at 65%, $\sigma = 0.20$ eV, $\Gamma = 0.25$ (0.50) eV. Ni(salen): D_{4h} symmetry, $[NiN_2O_2]$ site, $10Dq = 2.5$ eV, Slater integrals at 65%, $\sigma = 0.30$ eV, $\Gamma = 0.30$ (0.50) eV. $[Ni(cyclam)](ClO_4)_2$: D_{4h} symmetry, $[NiN_4]$ site, $10Dq = 3.0$ eV, Slater integrals at 65%, $\sigma = 0.25$ eV, $\Gamma = 0.25$ (0.50) eV. $(Ph_4As)_2[Ni(NCS)_4]$: D_{2d} symmetry, $[NiN_4]$ site, $10Dq = -0.6$ eV, $Ds = -0.15$ eV, Slater integrals at 60%, $L{\cdot}S_{3d}$ is at 60% (50 meV) of the calculated value, $\sigma = 0.25$ eV, $\Gamma = 0.20$ (0.35) eV. Ni-substituted rubredoxin: D_{2d} symmetry, $[NiS_4]$ site, $10Dq = -0.6$ eV, $Ds = -0.15$ eV, Slater integrals at 45%, $L{\cdot}S_{3d}$ is at 60% (50 meV) of the calculated value, $\sigma = 0.30$ eV, $\Gamma = 0.20$ (0.40) eV.

Fluorescence vs Electron Yield Spectra. The most commonly used method of measuring soft X-ray absorption spectra of 3d transition metal $L_{2,3}$ edges in solids is total electron yield, in which all escaping secondary electrons following Auger decay of the 2p core hole are recorded.[24] Probing depths for total electron yield in low-Z materials are typically a few hundred angstroms. Instead of total electron yield, photon detection after fluorescence decay of the core hole can also be used.[25] Since the photon created in the fluorescence decay has a mean free path length similar to the absorbed photon, for the fluorescence signal to be linearly proportional to the absorption cross section, a sample must be either spectroscopically thin or dilute. Otherwise, large saturation effects occur. In the limit that the only absorption process is at the transition metal $L_{2,3}$ edge, all photons above the threshold are eventually absorbed in a thick sample and contribute to the fluorescence yield signal. In this case the fluorescence intensity is not directly proportional to the absorption cross section and the highest peaks are compressed. Besides these saturation effects we can also have true "self-absorption" effects for the outgoing fluorescence photons, because the Ni $L_{2,3}$ edge fluorescence photon energy is very close to the absorption energy.[26] Depending on the fluorescence energy, the absorption coefficient of the outgoing photon will change, complicating the spectral shape further. Despite these problems, fluorescence yield is well suited for the measurement of dilute impurities,

(9) Kuiper, P.; Kruizinga, G.; Ghijsen, J.; Sawatzky, G. A.; Verweij, H. *Phys. Rev. Lett.* **1989**, *62*, 221–224.
(10) van Elp, J.; Searle, B. G.; Sawatzky, G. A.; Sacchi, M. *Solid State Commun.* **1991**, *80*, 67–71.
(11) Chemical abbreviations used are as follows: tren, tris(2-aminoethyl)-amine; ttcn, 1,4,7-trithiacyclononane; cyclam, 1,4,8,11-tetraazacyclodecane; salen, *N,N'*-ethylenebis(salicylideneaminato).
(12) Colpas, G. J.; Kumer, M.; Day, R. O.; Maroney, M. J. *Inorg. Chem.* **1990**, *29*, 4779–4788.
(13) Setzer, W. N.; Ogle, C. A.; Wilson, G. S.; Glass, R. S. *Inorg. Chem.* **1983**, *22*, 266–271.
(14) Barefield, E. K.; Wagner, F.; Flerlinger, A. W.; Dahl, A. R. *Inorg. Synth.* **1976**, *16*, 220.
(15) Steward, J. M.; Lingerfelter, E. C.; Breazeale, J. O. *Acta Crystallogr.* **1961**, *14*, 888–891.
(16) Forster, D.; Goodgame, D. M. L. *Inorg. Chem.* **1965**, *4*, 823–829.
(17) Ito, T.; Sugimoto, M.; Toriumi, K.; Ito, H. *Chem. Lett.* **1981**, 1477–1478.
(18) Blake, P. R.; Park, J.-B.; Bryant, F. O.; Aono, S.; Magnuson, J. K.; Eccleston, E.; Howard, J. B.; Summers, M. F.; Adams, M. W. W. *Biochemistry* **1991**, *30*, 10885–10895.
(19) Huang, Y.-H.; Moura, I.; Moura, J. J. G.; LeGall, J.; Park, J.-B.; Adams, M. W. W.; Johnson, M. K. *Inorg. Chem.* **1993**, *32*, 406–412.
(20) Chen, C. T.; Sette, F. *Rev. Sci. Instrum.* **1989**, *60*, 1616–1621.
(21) Cramer, S. P.; Chen, J.; George, S. J.; van Elp, J.; Moore, J.; Tensch, O.; Colaresi, J.; Yocum, M.; Mullins, O. C.; Chen, C. T. *Nucl. Instum. Methods* **1992**, *A319*, 285–289.
(22) Griffith, J. S. *The Theory of Transition-Metals Ions*; Cambridge University Press: New York, 1971.
(23) de Groot, F. M. F.; Fuggle, J. C.; Thole, B. T.; Sawatzky, G. A. *Phys. Rev. B* **1990**, *41*, 928–937.
(24) Gudat, W.; Kunz, C. *Phys. Rev. Lett.* **1972**, *29*, 169–172.
(25) Jaklevic, J.; Kirby, J. A.; Klein, M. P.; Robertson, A. S.; Brown, G. S.; Eisenberger, P. *Solid State Commun.* **1977**, *23*, 679–682.
(26) Wassdahl, N.; Bleckert, P.; Bray, G.; Glans, P.; Mårtensson, N.; Nordgren, J.; Rubinesson, J.-E.; Nyholm, R.; Cramm, S. X-ray and Innershell Processes. *AIP Conf. Proc.* **1990**, *215*, 451–464.

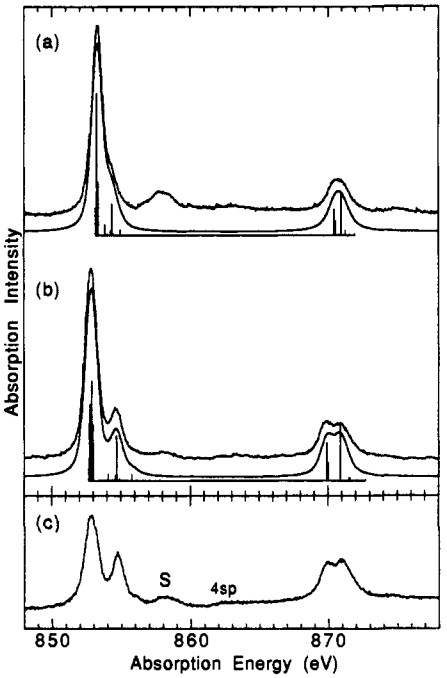

Figure 1. (a) Electron yield spectrum of $[Ni(ttcn)_2](BF_4)_2$ (top) compared with the calculated Ni^{2+} absorption spectrum (bottom) in O_h symmetry. (b) Electron yield spectrum of $[Ni(tren)_2](BF_4)_2$ (top) compared to the calculated Ni^{2+} absorption spectrum (bottom) in O_h symmetry. (c) Fluorescence yield spectrum of $[Ni(tren)_2](BF_4)_2$. Note the large difference in intensities between the electron yield and fluorescence yield spectra of $[Ni(tren)_2](BF_4)_2$, showing the large saturation effects and self-absorption effects present. The labels stand for (S) satellite structure and (4sp) start of the continuum absorption. The vertical lines below the calculations represent the positions and intensities of the individual transitions before line broadening.

because of the large escape depth and the elemental specificity of the fluorescence photon. For dilute materials the measured fluorescence intensity is equivalent to the absorption cross section[25] if the background absorption (μ_b) dominates the absorption at the Ni $L_{2,3}$ edges (μ_{Ni}), as is the case for most Ni-containing metalloproteins ($\mu_b \gg \mu_{Ni}$). As explained above, for concentrated materials, peaks are compressed; but if fluorescence yield detection is available, it is still very useful, because all the weak features in the electron yield data are enhanced in the fluorescence spectrum. With its bulk sensitivity, features absent in the fluorescence spectrum but present in the total electron yield spectrum suggest that these particular features are related to the surface, making fluorescence yield an easy probe for checking for surface degradation of the measured Ni model compounds.

Results and Discussion

Before we start a detailed analysis of our data, we will first briefly discuss the spectral features of a representative Ni $L_{2,3}$ edge spectrum. Typical spectra of $[Ni(ttcn)_2](BF_4)_2$ and $[Ni(tren)_2](BF_4)_2$ are shown in Figure 1a,b. The 2p spin–orbit interaction splits the spectrum into two parts, the L_3 ($2p_{3/2}$) edge at about 853 eV and the L_2 ($2p_{1/2}$) edge at about 870 eV. Both edges show sharp structures, with most of the spectral weight in the L_3 edge. In the fluorescence-detected spectrum of $[Ni(tren)_2](BF_4)_2$ (see Figure 1c) we can clearly identify two rather weak features, a satellite feature marked S, and the onset of the continuum 4sp band (labeled 4sp) reached by transitions to 4s states. The absorption at the L_3 edge, however, is much stronger than the absorption to the 4sp continuum states.

To explain the main line $L_{2,3}$ edge features, we have used an analysis based on an atomic multiplet calculation, with the inclusion of an adjustable ligand field splitting of the 3d orbitals to describe the local nickel symmetry. The actual calculation is for a $3d^8$ initial state to $\underline{2p}3d^9$ final states. The bottom of Figure 1a,b shows the theoretical results for both compounds. The Ni

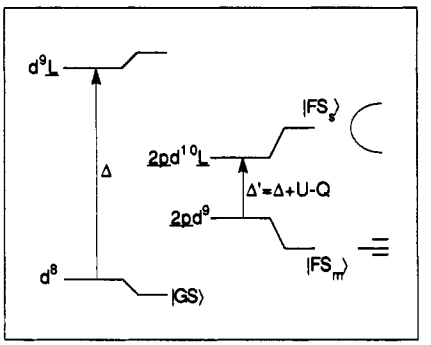

Figure 2. Schematic diagram of the energy levels of the initial state and the final states in the Ni^{2+} $L_{2,3}$ edge X-ray absorption process with the energy difference Δ between the d^8 and $d^9\underline{L}$ initial-state configurations and Δ' between the $\underline{2p}d^9$ and $\underline{2p}d^{10}\underline{L}$ final-state configurations. The broadening of the satellite is a result of the ligand hole bandwidth, as schematically shown at the top right of the figure. The main line obtains its width mostly from the $\underline{2p}d^9$ multiplet structure; shown are three final-state lines at the bottom right of the figure. The energy levels and final-state intensities are not to scale.

$L_{2,3}$ edges are special because there are no 3d–3d Coulomb and exchange interactions in the final states, due to the single final state 3d hole. The detailed structure arises from multiplet splittings mainly from the 2p–3d Coulomb and exchange interactions and the ligand field splitting of the 3d orbitals ($10Dq$ in O_h symmetry). In the calculation we used reduced Slater integrals, which results in a reduction of the multiplet splittings on going to less electronegative, more covalent ligands, as has been discussed for the Ni dihalides, where a consistent change in spectral weight is observed.[8] This reduction of multiplet splittings is comparable to the reduced Racah B and C parameters used in the analysis of optical 3d–3d transitions.

To understand the satellite feature labeled S, we have to discuss the changes in hybridization between the initial and final states. The ground state of a divalent Ni compound without taking the atomic multiplet structure or the ligand field splitting into account can be written as $|GS\rangle = \alpha|d^8\rangle + \beta|d^9\underline{L}\rangle$ with a charge-transfer energy Δ between the d^8 and $d^9\underline{L}$ (where $\underline{L}$ stands for a hole in the ligand band) energy levels (see Figure 2). The two final states available at the L_3 edge are $\underline{2p}d^9$ and $\underline{2p}d^{10}\underline{L}$, with a difference in energy $\Delta' = \Delta + U - Q$. Here U is the Mott–Hubbard Coulomb interaction between 3d electrons and Q is the Coulomb interaction between the 2p core hole and the 3d electrons.[8] The corresponding wave functions after hybridization are for the main line and satellite line respectively: $|FS_m\rangle = \alpha'|\underline{2p}d^9\rangle + \beta'|\underline{2p}d^{10}\underline{L}\rangle$ and $|FS_s\rangle = \beta'|\underline{2p}d^9\rangle - \alpha'|\underline{2p}d^{10}\underline{L}\rangle$. The intensity of the satellite is then given by[8] $I_s = (\sqrt{2}\alpha\beta' - \beta\alpha')^2$. Neglecting the $\sqrt{2}$, the satellite structure will only receive spectral weight if there is a change of hybridization in the final states as compared to the ground state (Δ' as compared to Δ, assuming transfer integrals stay the same). The values of Q and U are not very sensitive to the ligands, and for the Ni dihalides values around 7 and 5 eV are found, respectively.[8,27] The change of hybridization is not very large, Δ' is still positive and smaller than Δ, resulting in a small satellite intensity. The satellite feature marked S is identified as final states of mainly $\underline{2p}d^{10}\underline{L}$ character. The energy width of this feature depends on the hybridization with the empty 3d orbitals of e_g symmetry.

An important factor for an interpretation of the Ni $L_{2,3}$ edges is the effect of the ligand field on the 3d orbital energies. In O_h symmetry the 3d orbitals are split into e_g ($d_{x^2-y^2}$ and d_{z^2}) and t_{2g} (d_{xy}, d_{xz}, and d_{yz}) orbitals with an energy difference $10Dq$. The degenerate e_g orbitals have the highest energy and contain both the holes with parallel spin, to gain exchange energy stabilization. In both spectra shown in Figure 1, the ligand symmetry around

(27) Zaanen, J.; Westra, C.; Sawatzky, G. A. *Phys. Rev. B* **1986**, *33*, 8060–8073.

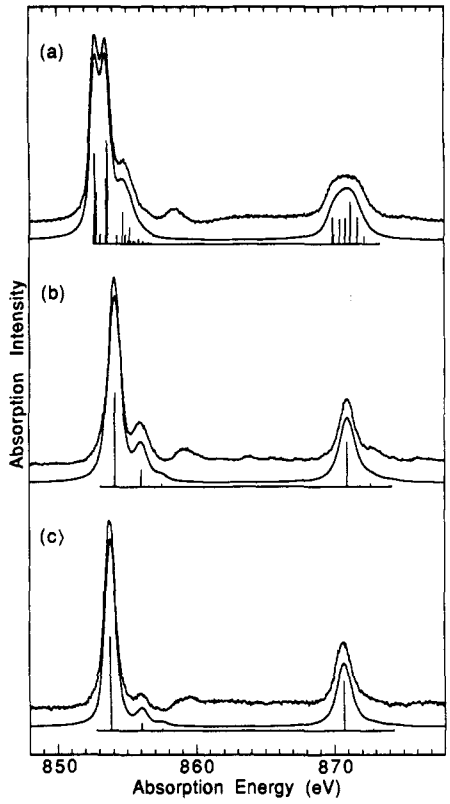

Figure 3. Ni $L_{2,3}$ edge spectra for Ni in D_{4h} symmetry: (a) Ni(cyclam)-Cl_2, (b) Ni(salen), (c) $[Ni(cyclam)](ClO_4)_2$. The top of each figure shows the experimental spectra, and the bottom the calculated Ni^{2+} absorption spectra. Ni(cyclam)Cl_2 has a high-spin ground state, while the bottom two spectra (b and c) show low-spin Ni^{2+} spectra. The vertical lines represent the positions and intensities of the individual transitions before line broadening.

the Ni atom is distorted O_h. In the $[Ni(tren)_2](BF_4)_2$ spectrum the L_3 and L_2 edges are both split into double-peaked features, which are comparable to the spectral features of Ni oxalate.[7] The satellite feature (mainly $\underline{2p}d^{10}\underline{L}$ final states) is rather weak and separated from the main line multiplet structure, as compared to the Ni dihalides, where the satellite structure overlays the main line multiplet structure.[8] In $[Ni(ttcn)_2](BF_4)_2$ (Figure 1a) we see a very distinct splitting of the satellite structure. As in NiI_2,[8] the multiplet structure in the $L_{2,3}$ edges of $[Ni(ttcn)_2](BF_4)_2$ is weaker due to the increased covalency of the sulfur ligands, compared to the nitrogen ligands of $[Ni(tren)_2](BF_4)_2$. Only a low-intensity, high-absorption energy shoulder is left at the L_3 edge. The strongly reduced Slater integrals used in the calculations for $[Ni(ttcn)_2](BF_4)_2$ are reflected in the smaller multiplet splittings observed. The Slater integrals used in the calculations for $[Ni(ttcn)_2](BF_4)_2$ are at the limit of the assumption that the ground state can be described as mainly having d^8 character or, said differently, that an ionic Ni^{2+} (d^8) is a good starting point for $[Ni(ttcn)_2](BF_4)_2$.

In Figure 3 we show spectra obtained from Ni compounds with D_{4h} symmetry. In D_{4h} geometry the $d_{x^2-y^2}$ orbital is directed toward the equatorial ligands, which results quite often in a singlet low spin ground state. This is however not the case for Ni(cyclam)-Cl_2, where the ground state remains high spin. The Ni(cyclam)-Cl_2 spectrum (Figure 3a) shows two strong peaks (split by about 800 meV), with a distinctive shoulder at the L_3 edge and a very broad structure at the L_2 edge. A similar splitting into two peaks at the L_3 edge is observed[28] for stochiometric La_2NiO_4 where Ni is also in a D_{4h} symmetry, with the two apical oxygen atoms at a much longer distance. In Ni(cyclam)Cl_2 it is the combination of Cl atoms on the z-axis, as compared to the in-plane N atoms, and the longer apical distance of the Cl atoms which splits the e_g and t_{2g} orbitals. The ground state is, however, still high spin ($^3B_1$ symmetry in D_{4h}, with minority spin $d_{x^2-y^2}$ and d_{z^2} orbitals empty), and the spectrum is quite different from the low-spin spectra of Figure 3b,c and the O_h spectra of Figure 1. In D_{4h} geometry we have two new ligand field parameters Ds and Dt describing the distortion. By using Ds in the calculation for Ni-(cyclam)Cl_2, we leave the center of energy for the e_g- and t_{2g}-derived orbitals the same but split the e_g orbitals by $4Ds$ into $d_{x^2-y^2}$ (b_1 in D_{4h} symmetry) and d_{z^2} (a_1) and the t_{2g} by $3Ds$ into d_{xy} (b_2) and d_{xz},d_{yz} (e). Values of Ds = 220 meV and $10Dq$ = 1.6 eV are used in the calculation. Similar values for $10Dq$ (1.8 eV) and the splitting of the e_g states is found from a study in the optical region.[29] The splitting between the two peaks in the main line of the L_3 edge in D_{4h} symmetry is comparable but not equal to $4Ds$.

The combination of ligand field distortion and 3d valence band spin–orbit coupling in D_{4h} symmetry splits the $^3A_{2g}$ (O_h) symmetry ground state into an $m_s = 0$ state and a doubly degenerate $m_s = \pm 1$ state at a slightly higher energy (<0.1 meV). The calculated spectrum from the $m_s = 0$ state has more spectral weight at the first peak of the double-peaked L_3 edge structure, while the $m_s = \pm 1$ state shows more spectral weight at the second peak. Also, the $m_s = \pm 1$ spectrum has of course, in total, twice the spectral weight. We find no difference between spectra taken at 10 and 300 K, indicating that both states are populated at 10 K and that the zero field splitting is small, as compared to kT at 10 K.

The two low-spin D_{4h} Ni site symmetry spectra are shown in Figure 3b,c. Both have sharp peaks at the L_3 and L_2 edges, followed at the L_3 edge by a weaker peak at higher absorption energy in Ni(salen). The absorption energy of the low-spin L_3 edge is at higher energy than the high-spin L_3 edge energy position. The large difference compared to the Ni(cyclam)Cl_2 high-spin spectrum with similar D_{4h} symmetry is a direct result of the different ground state and a different subset of final states (only $\underline{2p}$ coupled to mainly b_1) allowed in the absorption process. The ground state is an $^1A_1$ symmetry with mainly both spin up and spin down $d_{x^2-y^2}$ orbitals unoccupied. The theoretical spectra in Figure 3b,c are calculated by choosing the D_{4h} parameters such[7] that the b_2, a_2, and e 3d orbital energies are degenerate at an energy $10Dq$ below b_1 ($Ds = 10Dq/7$ and $Dt = 6Dq/7$), which is a reasonable assumption for low-spin Ni^{2+}. The L_3 higher absorption energy peak is obtained from the 2p core hole coupled to b_2, a_2, and e symmetry empty 3d orbitals. The intensity is quite sensitive to the value of $10Dq$,[7] as shown in Figure 3c, where we used a value of $10Dq$ = 3.0 eV for $[Ni(cyclam)](ClO_4)_2$, as compared to $10Dq$ = 2.5 eV for Ni(salen). In the low-spin calculations the branching ratio ($L_3/(L_3 + L_2)$) decreases with increasing $10Dq$ and is overall significantly smaller then the high-spin branching ratio.[30]

In Figure 4 we show the spectra of $(Ph_4As)_2[Ni(NCS)_4]$ and the Ni-substituted *P. furiosus* rubredoxin. In both spectra we find at the high absorption energy side of the L_3 edge a broad satellite structure of mainly $\underline{2p}d^{10}\underline{L}$ character overlapping the main L_3 edge features. The actual symmetries of the two systems are distorted tetrahedral. A nondistorted T_d symmetry calculation with $10Dq$ = –0.6 eV is shown in Figure 4b. Clearly, the intensity and the shape of the L_2 edge is different from the experimental spectra. Different $10Dq$ values in the T_d symmetry calculations show little effect on the shape and intensity of the L_2 edge.[5] The Ni^{2+} ground state in T_d symmetry is $^3T_1$ (^3F), with one minority spin t_{2g} orbital occupied. In the actual calculations we used a D_{2d} distortion which splits the 3d orbitals (T_d to D_{2d}) in a similar way as O_h to D_{4h}. With a Ds = –150 meV distortion, the L_2 edge gains some intensity and acquires the correct structural features. The D_{2d} distortion with a negative Ds lowers the energy of the d_{xy}

(28) Kuiper, P.; van Elp, J. Unpublished work.

(29) Martin, L. Y.; Sperati, C. R.; Busch, D. H. *J. Am. Chem. Soc.* **1977**, *99*, 2968–2981.

(30) Thole, B. T.; van der Laan, G. *Phys. Rev. B* **1988**, *38*, 3158.

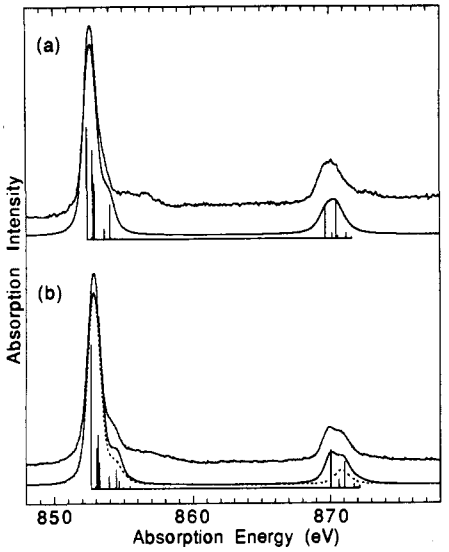

Figure 4. (a) Experimental Ni $L_{2,3}$ edge spectrum of the Ni-substituted *P. furiosus* rubredoxin (top) and the calculated absorption spectrum (bottom). (b) Experimental spectrum of $(Ph_4As)_2[Ni(NCS)_4]$ (top) and the calculated absorption spectrum in D_{2d} symmetry (bottom). The dashed line is a calculation in T_d symmetry with $10Dq = -0.6$ eV. The vertical lines represent the positions and intensities of the individual transitions before line broadening.

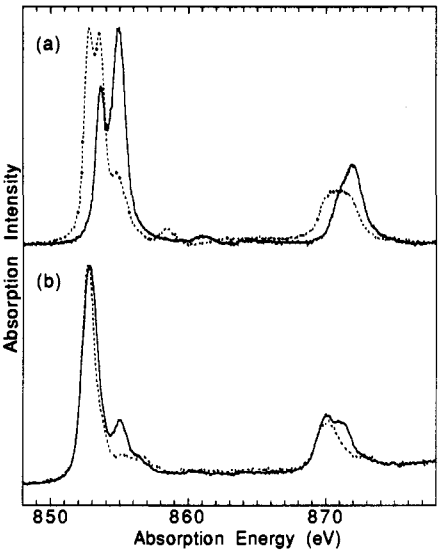

Figure 5. (a) Formally divalent Ni spectrum of Ni(cyclam)Cl_2 (dashed line) and the formally trivalent Ni spectrum of $[Ni(cyclam)Cl_2]ClO_4$ (solid line). (b) As-prepared form of the Ni-substituted *P. furiosus* rubredoxin (dashed line) and the 30% oxidized form (solid line).

orbital and raises the energy of the d_{xz} and d_{yz} orbitals, which therefore contain both 3d holes. More intensity at the L_2 edge is gained from lowering the valence band spin–orbit coupling to 50 meV (instead of the *ab initio* value of 83 meV).[31]

The spin–orbit coupling and the distortion from T_d symmetry create zero field splittings for the D_{2d} symmetry, which are for this particular symmetry very large. We find a doubly degenerate state ($m_s = \pm 1$) at 7.7 meV. In a temperature dependent optical magnetic circular dichroism study a zero field splitting pattern with a nondegenerate ground state and a double degenerate state at 7.6 meV (61 cm^{-1}) is found for the Ni-substituted *D. gigas* rubredoxin.[32] Similar values were found for the Ni-substituted rubredoxins of *D. vulgaris* and *C. pasteurianum*,[32] and 5.5 meV (44 cm^{-1}) for the distorted tetrahedral Ni center in $(Ph_4P)_2Ni(SPh)_4$.[32] A value of 9.4 meV (76 cm^{-1}) is reported[33] for the Ni-substituted *P. furiosus* rubredoxin. The calculated zero field splitting value is strongly dependent on the spin–orbit splitting and the D_{2d} distortion parameter (Ds). For the nitrogen-coordinated model $(Ph_4As)_2[Ni(NCS)_4]$ we found 8.0 meV. These values are reasonably close to the optical MCD values, taking into account that the zero field splittings are calculated using final-state parameters obtained from the absorption spectrum.

For both systems, the electronic distortions we find are large, indicating that besides the electronic distortions from T_d to D_{2d} symmetry there should also be a significant Ni local geometry distortion in the Ni-substituted *P. furiosus* rubredoxin and $(Ph_4As)_2[Ni(NCS)_4]$. The actual geometry of a similar T_d symmetry model complex, $(Ph_4P)_2Ni(SPh)_4$, shows a highly distorted $[NiS_4]$ core, with S–Ni–S angles ranging from 92.0° to 124.9°, that approaches D_{2d} symmetry.[34] Resonance Raman spectra indicate a tetragonally elongated tetrahedral $[NiS_4]$ core for the Ni-substituted *P. furiosus* rubredoxin.[35]

Not every electronic and geometric distortion shows up in the Ni $L_{2,3}$ edge spectrum. Starting from the O_h symmetry, the D_{3d} distortion[36] splits the t_{2g} states into a_1 and e symmetry, but the e_g states remain degenerate (e symmetry). The states of e symmetry will mix with each other. With $10Dq = 1.5$ eV and splittings of 600 meV for the t_{2g} states the calculated spectra show only minor changes, changes mostly due to small splittings in the final states. The difference with D_{4h} symmetry is that the two empty 3d orbitals are split in energy because of the distortion, while in D_{3d} symmetry the two empty orbitals stay degenerate, so that we find only minor final-state energy changes as compared to D_{4h}. In D_{3d} the ground state also splits into a nondegenerate $m_s = 0$ level and a doubly degenerate $m_s = \pm 1$ level, with splittings large enough to show a temperature dependence in the Ni $L_{2,3}$ edge spectra.

The $L_{2,3}$ edge absorption spectra are also sensitive to oxidation-state changes, and in Figure 5 we show the results upon oxidation of two Ni complexes. The local Ni geometry changes slightly upon oxidation of $[Ni(cyclam)Cl_2]$; distances for the formally divalent Ni^{14} of Ni–N 2.06 Å and Ni–Cl 2.50 Å change to Ni–N 1.97 Å and Ni–Cl 2.45 Å for the formally trivalent Ni^{17} at the $[NiN_4Cl_2]$ site. Besides the totally different shape of the spectrum, in $[Ni(cyclam)Cl_2]ClO_4$ the absorption energy position has shifted to higher energy. In $Li_xNi_{1-x}O$[10] the absorption energy position does not change upon doping. In Figure 5b we show the Ni-substituted *P. furiosus* rubredoxin as prepared and 30% ferricyanide oxidized with excess cyanide. A profound change in the spectrum upon partial oxidation is also observed for the Ni-substituted *P. furiosus* rubredoxin. We see a new feature at an absorption energy of 855 eV in the L_3 edge, and at the L_2 edge a strong increase in intensity at the high-energy side. Both features are directly related to the oxidized form.

In the last few years there has been renewed spectroscopic interest in hole-doped Ni^{2+} systems because of the discovery of the Cu-based high-T_c superconductors. The charge-compensating states upon hole doping in $Li_xNi_{1-x}O$[9,10] and $La_{2-x}Sr_xNiO_4$[37] were shown to be of primarily O 2p character. The ground state in these two systems for the end members upon doping (Ni^{3+}) is mainly $d^8\underline{L}$, so from the three holes one hole is delocalized onto the oxygen neighbors. The delocalized hole, however, has 3d orbital symmetry.

The conclusion that the charge-compensating hole is mainly localized on the ligands is partly based on the inability to reproduce

(31) van der Laan, G.; Thole, B. T. *Phys. Rev. Lett.* **1988**, *60*, 1977–1980.
(32) Kowal, A. T.; Zambrano, I. C.; Moura, I.; Moura, J. J. G.; LeGall, J.; Johnson, M. K. *Inorg. Chem.* **1988**, *27*, 1162–1166.
(33) Huang, Y.-H. Ph.D. dissertation, University of Georgia, 1992.
(34) Svenson, D.; Baenziger, N. C.; Coucouvanis, D. *J. Am. Chem. Soc.* **1978**, *100*, 1932–1934.
(35) Huang, Y.-H.; Moura, I.; Moura, J. J. G.; LeGall, J.; Park, J.-B.; Adams, M. W. W.; Johnson, M. K. *Inorg. Chem.* **1993**, *32*, 406–412.
(36) Ballhausen, C. J. *Introduction to Ligand Field Theory*; McGraw-Hill, New York, 1962.
(37) Kuiper, P.; van Elp, J.; Sawatzky, G. A.; Fujimori, A.; Hosaya, S.; de Leeuw, D. M. *Phys. Rev. B* **1991**, *44*, 4570–4575.

the Ni $L_{2,3}$ edges for the trivalent end members. This has been shown for the $Li_xNi_{1-x}O$ system,[9,10] but is also true for the trivalent $[Ni(cyclam)Cl_2]ClO_4$. In the present calculations an ionic approximation (that Ni^{2+} is truly d^8) is made, and covalency is taken into account by a reduction of the Slater integrals. Despite the covalency, the lowest energy configuration for Ni^{2+} is still d^8, with $d^9\underline{L}$ at a charge-transfer energy Δ. This allows us to describe the Ni $L_{2,3}$ edge for a divalent Ni compound as a d^8 to $2pd^9$ transition. The ground state of a trivalent Ni compound is a mixture of d^7, $d^8\underline{L}$, and $d^9\underline{L}^2$, and to be able to describe the trivalent Ni $L_{2,3}$ edge as a d^7 to $\underline{2p}d^8$ transition, the lowest configuration should be d^7 and not $d^8\underline{L}$. If we compare the $[Ni(cyclam)Cl_2]ClO_4$ $L_{2,3}$ edge spectrum with our calculations and published calculations[5,10] of Ni^{3+} in low spin, it becomes clear that even with strongly reduced Slater integrals the experimental data cannot be described using a calculation with an ionic trivalent d^7 starting point, suggesting that the lowest configuration is $d^8\underline{L}$ and not d^7. Therefore, the ground state for the covalent $[Ni(cyclam)Cl_2]ClO_4$ compound is of mainly $d^8\underline{L}$ character, with one of the three holes delocalized onto the ligands.

A similar result[38] is also found for the formally tetravalent Fe in $SrFeO_3$, where the Fe 2p absorption spectra cannot be reproduced with calculations starting with a d^4 (tetravalent Fe) initial state. In both the two shown Ni systems, the Ni $L_{2,3}$ edge spectral features, although they cannot be described with d^7 to $\underline{2p}d^8$ calculations, do change upon oxidation.

Conclusions

The current work shows how structural changes at the Ni site affect the electronic structure and corresponding $L_{2,3}$ edge X-ray absorption spectra. We conclude that the Ni $L_{2,3}$ edge is very sensitive to both the oxidation state (divalent Ni versus trivalent Ni) and the spin state (low-spin Ni^{2+} versus high-spin Ni^{2+}). The $L_{2,3}$ edges show, when the ionic approximation of d^n for the initial state is appropriate, a "fingerprint" of final-state multiplet structure in the absorption spectrum for every d^n to $2pd^{n+1}$ transition. Although the "fingerprint" of d^7 is not visible in the formally trivalent Ni compounds, the spectral features do change upon oxidation. This is clear in the two examples we have shown, the Ni-substituted rubredoxin and the Ni cyclam structure, but is also found for rare earth nickel perovskites[39] as compared to NiO and in Li-doped NiO.[10] High-spin or low-spin Ni sites also show a large difference in their spectral features.

Secondly, the Ni $L_{2,3}$ edge is sensitive to different structural Ni site symmetries. Differences in the main spectral features can be explained with a change in electronic structure based on the molecular structure. Most strongly visible at the $L_{2,3}$ edges is the splitting of the e_g orbitals in the high-spin D_{4h} symmetry, as observed in $Ni(cyclam)Cl_2$. However, since it is electronic structure that produces the change in spectral features, Ni $L_{2,3}$ edges can only detect structural differences that change electronic structure. If the 3d splittings are the same in two different structures (for instance removing a ligand from a D_{4h} structure to create a square pyramidal C_{4v} symmetry), we can expect to see comparable Ni $L_{2,3}$ edge spectra, with perhaps small changes due to different hybridization strengths.

Finally, Ni $L_{2,3}$ edges are also sensitive to the type of ligands present. As the ligands become more covalent, the observable multiplet splittings decrease. This is comparable to the covalency effects which require reduction of the Racah B and C parameters.

As a biologically relevant test case, we have investigated Ni-substituted *P. furiosus* rubredoxin. We find that it has a strongly distorted T_d symmetry, which we described electronically by using a D_{2d} symmetry electronic structure. The zero field splitting deduced from the $L_{2,3}$ edges is large (7.7 meV or 62 cm^{-1}) and comparable to that obtained from an optical MCD study. The large electronic distortion indicates that the Ni site should have a strong structural distortion. Upon partial oxidation we find new features appearing in the $L_{2,3}$ edge spectrum. Other Ni-containing proteins such as hydrogenase and CO dehydrogenase are also being studied by this technique.

Acknowledgment. We wish to thank L. H. Tjeng and H.-J. Lin for their help during the experiments. This work was supported by the National Science Foundation through Grants DMB-9011583 (to MWWA) and DMB-8921986 (to M.K.I.), the National Institutes of Health through GM-44380 (to S.P.C.) and GM-38829 (to M.J.M.), the Department of Energy, Office of Health and Environmental Research, and by Lawrence Berkeley Laboratory LDRD Exploratory Research Funds (to S.P.C.). The Center for Metalloenzyme Studies at the University of Georgia is funded by a grant from the National Science Foundation (DIR-9014281), and the National Synchrotron Light Source is supported by the Department of Energy, Office of Basic Energy Sciences.

(38) Abbate, M.; de Groot, F. M. F.; Fuggle, J. C.; Fujimori, A.; Strebel, O.; Lopez, F.; Domke, M.; Kaindl, G.; Sawatzky, G. A.; Takano, M.; Takeda, Y.; Eisaki, H.; Uchida, S. *Phys. Rev. B* **1992**, *46*, 4511–4519.

(39) Medarde, M.; Fontaine, A.; García-Munoz, J. L.; Rodríquez-Carvajal, J.; de Sanmtis, M.; Sacchi, M.; Rossi, G.; Lacorre, P. *Phys. Rev. B* **1992**, *46*, 14975–14984.